Efficient homogeneous electrochemical water oxidation catalysed by macrocyclic nickel complex with redox non-innocent pyridine coordination structure

Junqi Lin[a,*], Jinlin Hu[a], Zhichao Qi[a], Lianghui Zhang[a], Zezhen Wang[a], Xiangming Liang,[b,*] Zhijun Ruan[a,*]

[a] Hubei Key Laboratory of Processing and Application of Catalytic Materials, College of Chemistry and Chemical Engineering, Huanggang Normal University, Huanggang, 438000 China.

[b] School of Basic Medical Sciences, Ningxia Medical University, Yinchuan, 750004, China.

Email: linjunqi@hgnu.edu.cn, liangxm@nxmu.edu.cn, ruanzhijun87@126.com

Table S1 Crystallographic data and processing parameters for complex **1**

Complex parameters	$[Ni(Me_3pyclen)(CH_3CN)_2](ClO_4)_2$ (**1**)
Empirical formula	$C_{18}H_{30}Cl_2N_6NiO_8$
Formula weight	588.09
Temperature / K	293(2) K
Wavelength / Å	0.71073
Crystal system	monoclinic
Space group	$P2_1/c$
a / Å	8.9341(9)
b / Å	18.5476(14)
c / Å	15.7100(15)
α / deg	90
β / deg	90.057(3)
γ / deg	90
Volume / $Å^3$	2603.2(4)
Z	4
Calculated density / Mg m^3	1.501
Absorption coefficient	1.003 mm^{-1}
F(000)	1224
Crystal size / mm	0.3 × 0.28 × 0.26
2*θ* range / deg	4.392 to 50.132
Index ranges	-10<=h<=10, -20<=k<=22, -18<=k<=18
Reflections collected	28213
Independent reflections	4591 [R_{int} = 0.6389, R_{sigma} = 0.1701]
Completeness to theta = 24.792°	99.5 %
Absorption correction	Semi-empirical from equivalents
Refinement method	Full-matrix least-squares on F^2
Data / restraints / parameters	4591 / 254 / 404
Goodness-of-fit on F^2	1.076
Final R indices [I>2sigma(I)]	R_1 = 0.0996, wR_2 = 0.2424
R indices (all data)	R_1 = 0.1294, wR_2 = 0.2655
Largest diff. peak and hole	0.72 and -0.53 e.$Å^{-3}$

$R_1 = \Sigma||F_o| - |F_c||/\Sigma|F_o|$, $wR_2 = [\Sigma(|F_o|^2 - |Fc|^2)^2/\Sigma(Fo_2)]^{1/2}$

Table S2 Selected bond lengths (Å) and angles (deg) for complex **1**

Complex	**1**	Bond angles (deg)	
Bond length (Å)		N1–Ni1–N2	79.7(3)
Ni1–N1	1.997(6)	N1–Ni1–N3	91.4(2)
Ni1–N2	2.147(7)	N1–Ni1–N4	80.9(3)
Ni1–N3	2.133(6)	N1–Ni1–N5	175.0(3)
Ni1–N4	2.161(7)	N1–Ni1–N6	87.9(3)
Ni1–N5	2.052(7)	N2–Ni1–N3	84.0(3)
Ni1–N6	2.105(8)	N2–Ni1–N4	157.1(3)
		N2–Ni1–N5	100.1(3)
		N2–Ni1–N6	95.2(3)
		N3–Ni1–N4	84.5(3)
		N3–Ni1–N5	93.5(3)
		N3–Ni1–N6	170.9(3)
		N4–Ni1–N5	100.2(3)
		N4–Ni1–N6	96.0(3)
		N5–Ni1–N6	87.2(3)

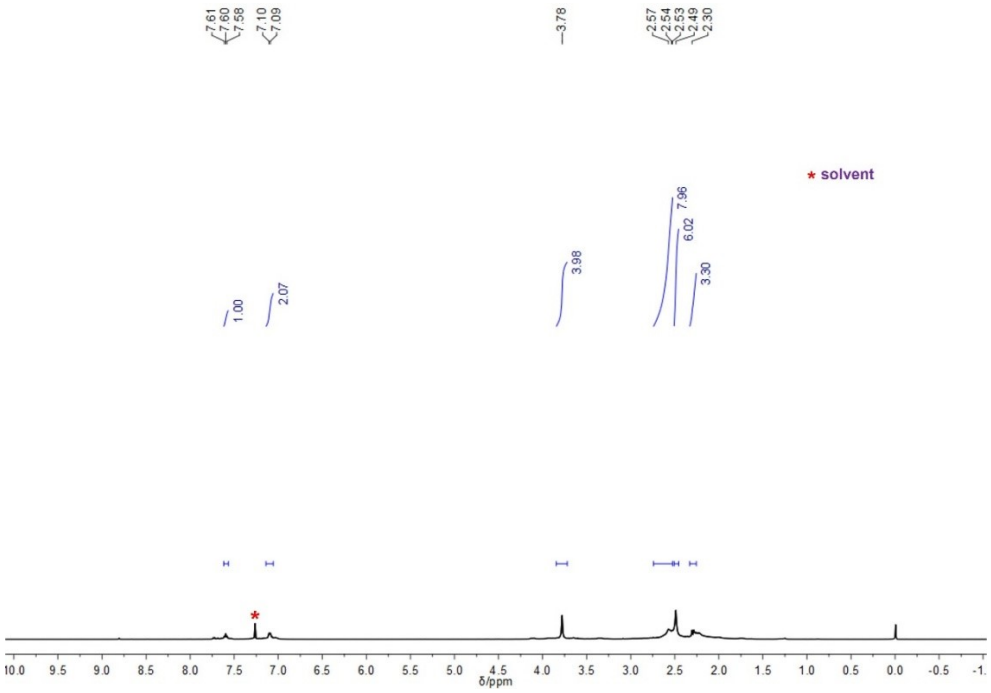

Fig. S1 The ^{1}H NMR (400 MHz, chloroform-*d*) of the ligand Me_3pyclen: δ 7.60 (t, 1H, CH_{py}), 7.10 (d, 2H, CHpy), 3.78 (s, 4H, CH_2), 2.54 (t, 8H, CH_2CH_2), 2.49 (s, 6H, CH_3), 2.90 (s, 3H, CH_3).

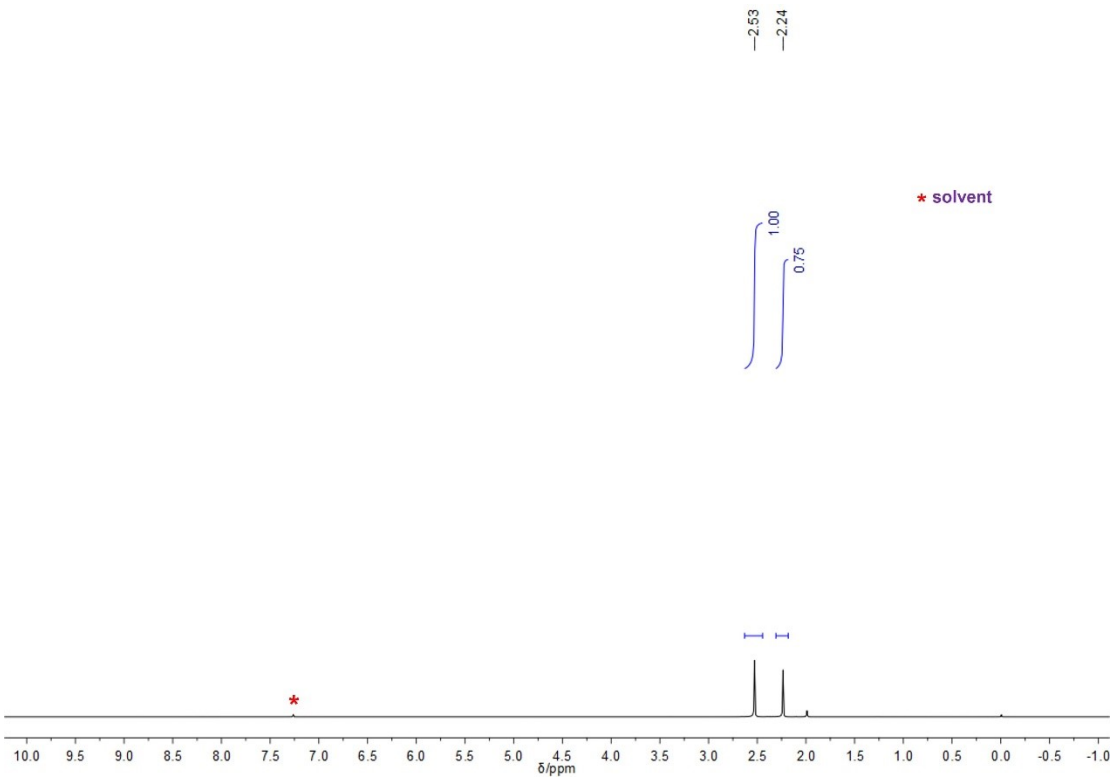

Fig. S2 The ^{1}H NMR (400 MHz, chloroform-*d*) of the ligand 12-TMC: δ 2.53 (s, 4H, CH_2CH_2), 2.24 (s, 3H, CH_3).

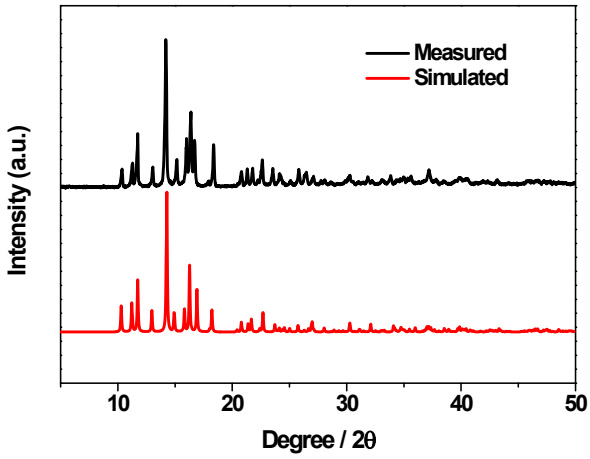

Fig. S3 Measured and simulated PXRD pattern of the as-synthesized sample of **2**.

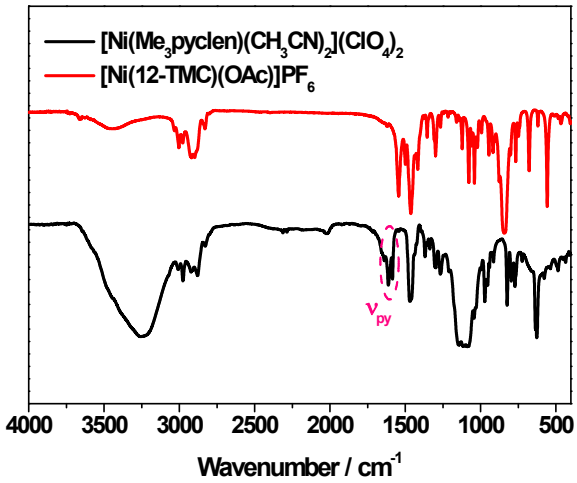

Fig. S4 FT-IR spectra of complexes **1** and **2**, the vibration at around 1600 cm^{-1} should be assigned to the signal of pyridine ring of the Me_3pyclen ligand.

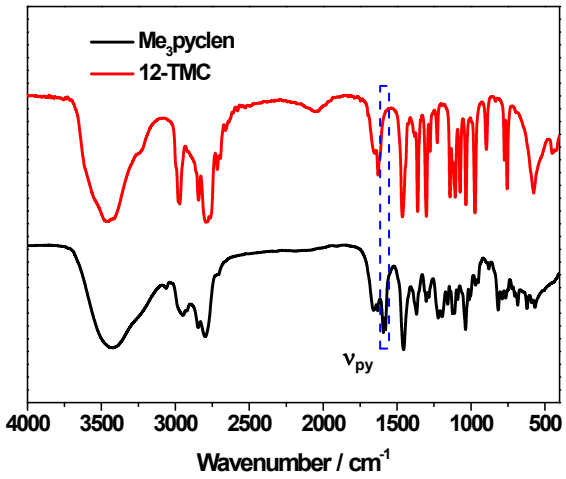

Fig. S5 The FT-IR spectra of the Me_3Pyclen ligand and the 12-TMC ligand.

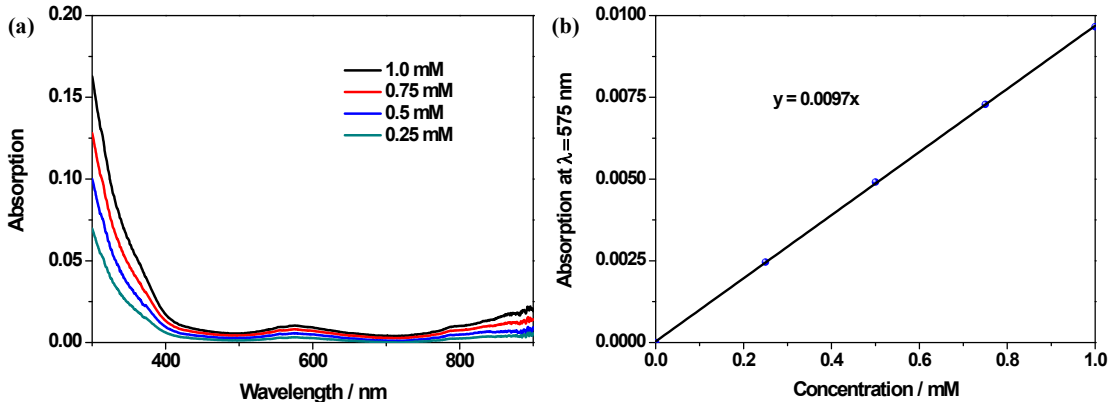

Fig. S6 (a) UV-vis absorption spectra of **1** with various concentrations. (b) Relationship between the absorption value of the characteristic peak at λ = 575 nm and concentration of **1**.

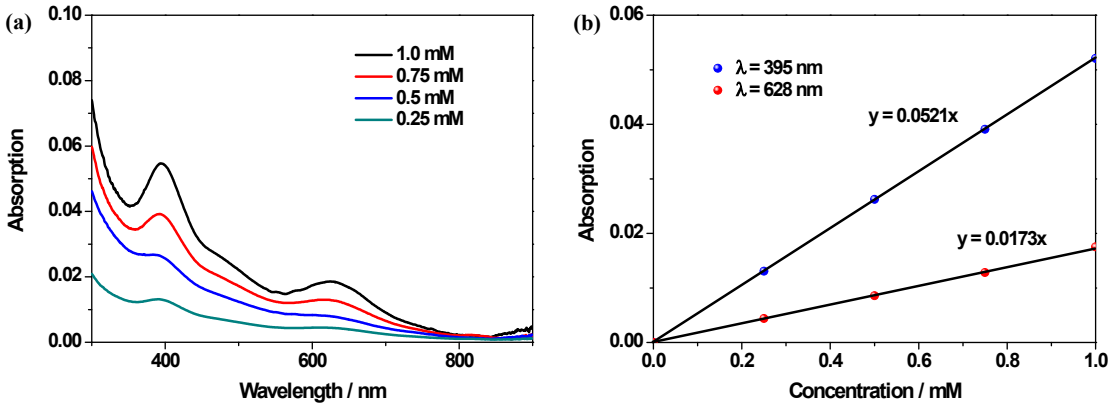

Fig. S7 (a) UV-vis absorption spectra of **2** with various concentrations. (b) Relationship between the absorption value of the characteristic peak at λ = 575 nm and concentration of **2**.

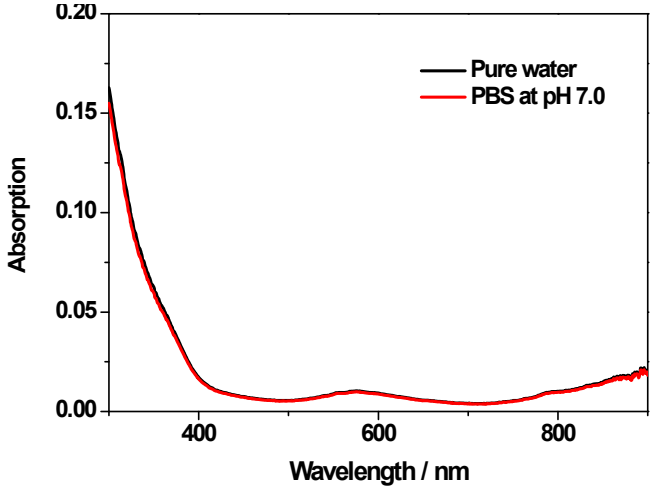

Fig. S8 UV-vis absorption spectra of 1.0 mM of **1** in pure water and PBS at pH 7.0.

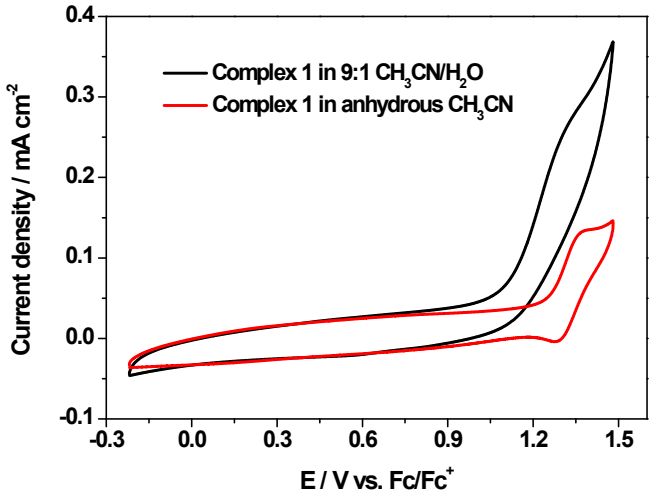

Fig. S9 The CV test of 1 mM of **1** in anhydrous CH_3CN and 95:5 CH_3CN/ H_2O mixed solvent with 0.1 M tetrabutylammonium hexafluorophosphate as electrolyte, scan rates = 100 mV s^{-1}.

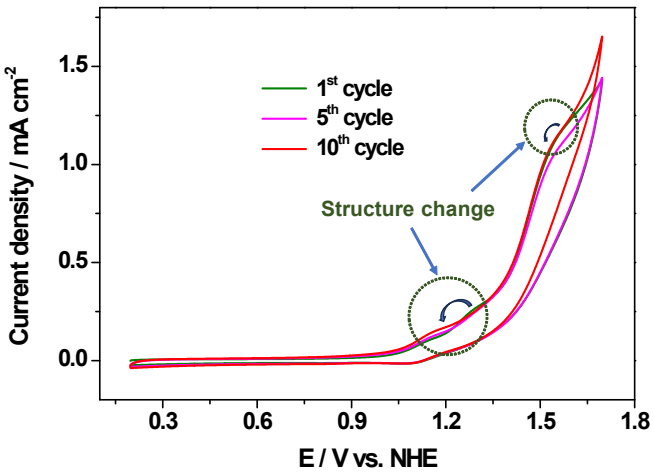

Fig. 10 The 1st, 5th, and 10th CV scan of 1 mM of **2** in 0.1 M PBS at pH 7.0, scan rate = 100 mV/s.

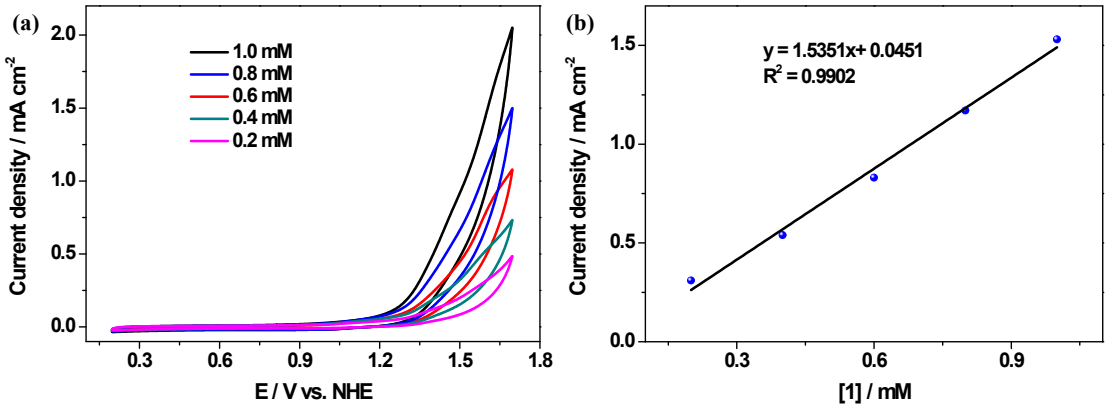

Fig. S11 CV of various concentrations of **1** in 0.1 M PBSs at pH 7.0 with scan rate of 100 mV s^{-1} (a). Dependence of catalytic current density of catalytic wave on the concentration of **1** (b).

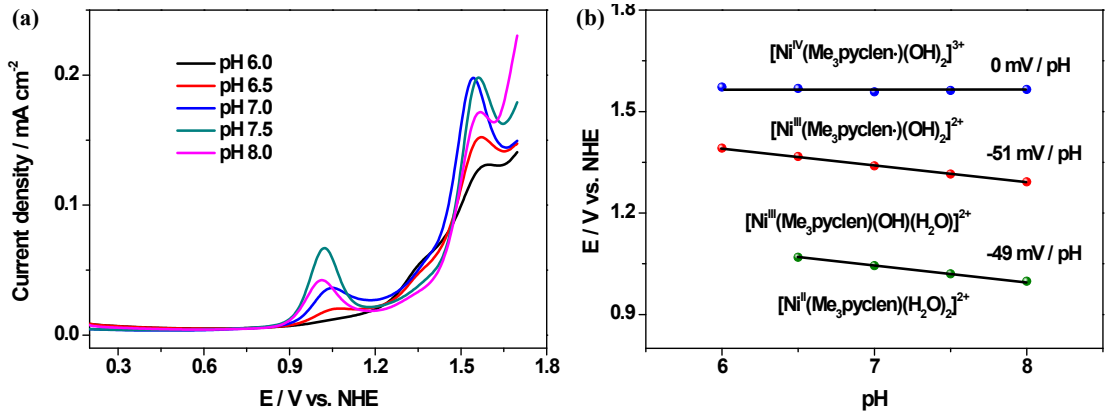

Fig. S12 DPV tests of 1 mM of **1** in 0.1 M PBS at various pH values (a) and the relationship between the potential of each redox couple of **1** and the pH value of electrolyte (b).

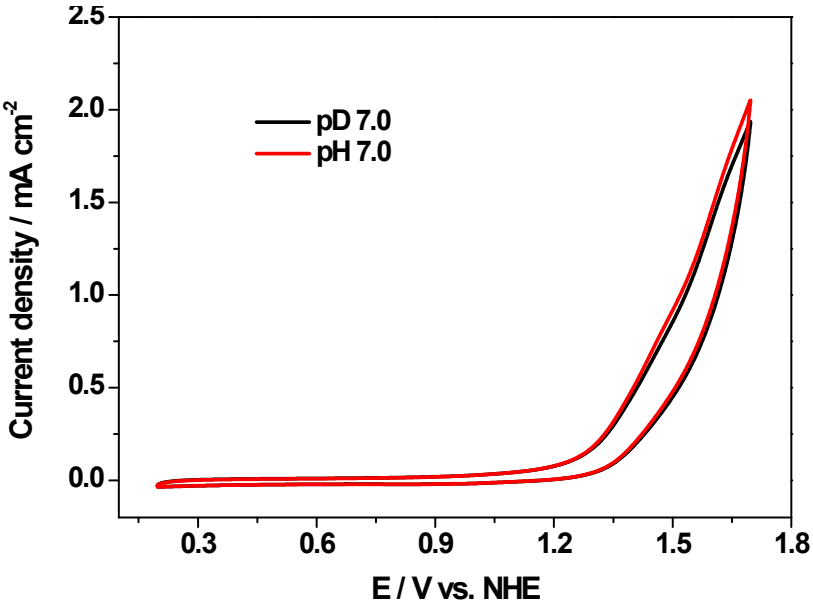

Fig. S13 CV tests of 1.0 mM of 1 in neutral PBS with H_2O and D_2O as solvent.

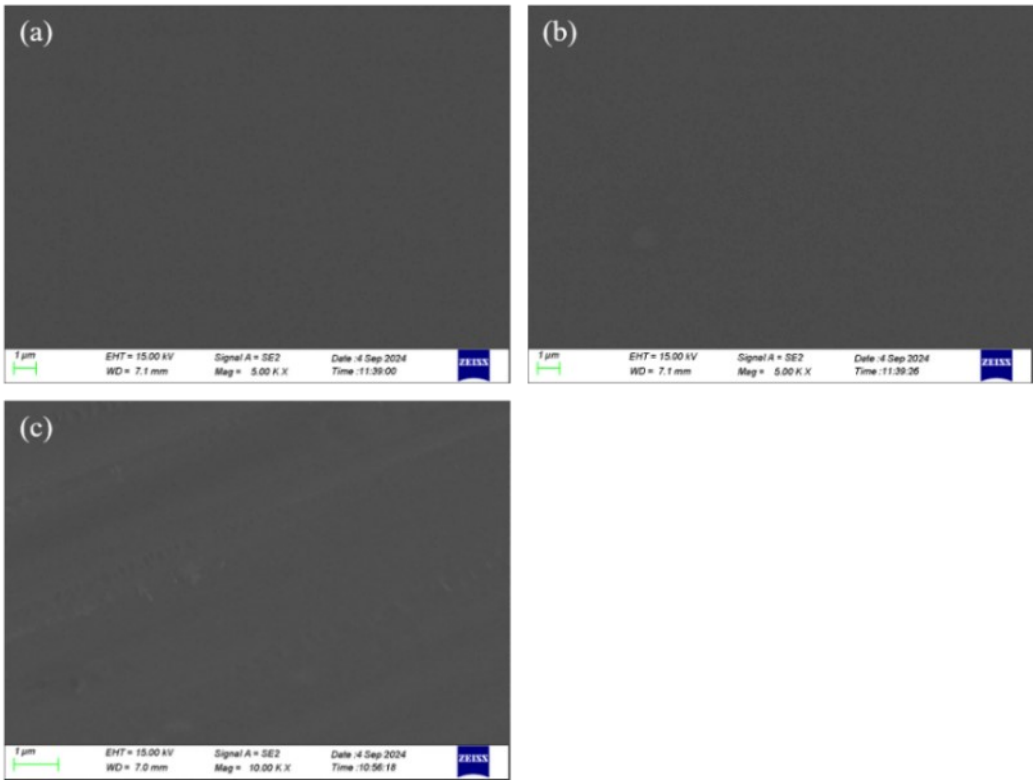

Fig. S14 Morphology of clean ITO electrode (a), post-CPE ITO-**1** (b) and post-CPE ITO-**2** (c).

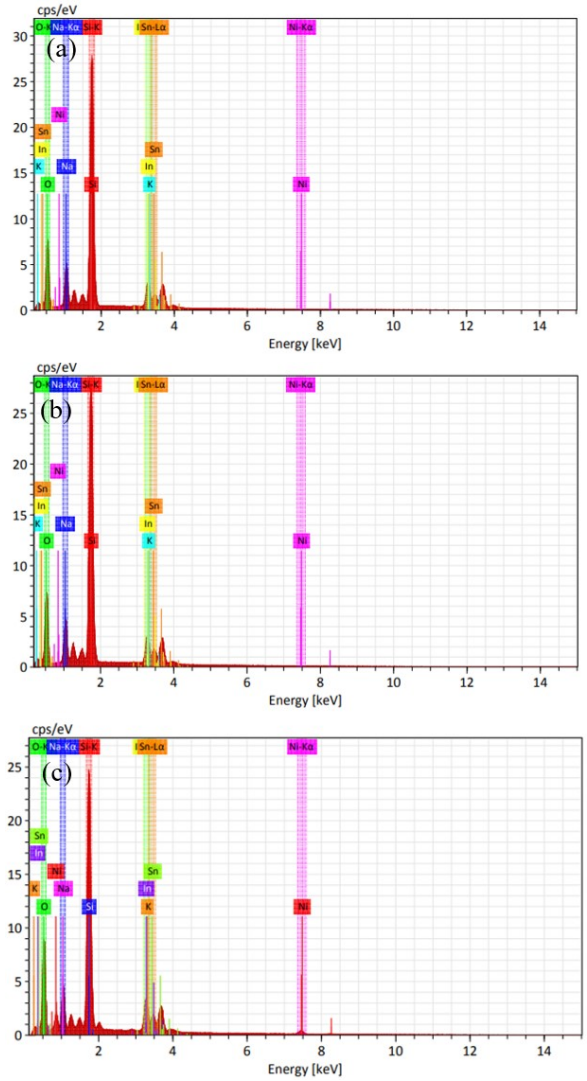

Fig. S15 EDS analysis on the surface of clean ITO electrode (a), post-CPE ITO-**1** (b) and post-CPE ITO-**2** (c).

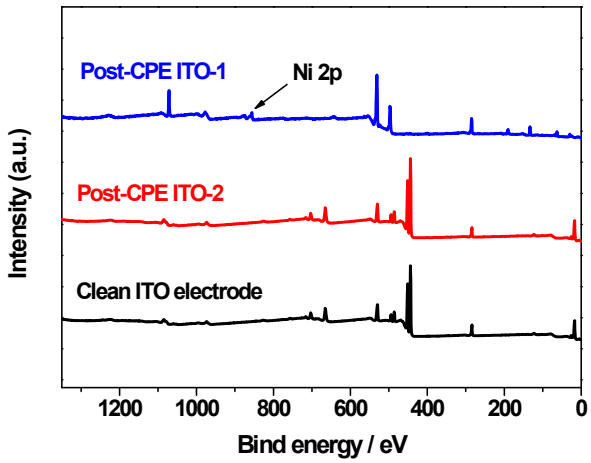

Fig. S16 Full XPS spectra of clean ITO electrode, post-CPE ITO electrode. The binding energy has been calibrated by the C 1s peak.

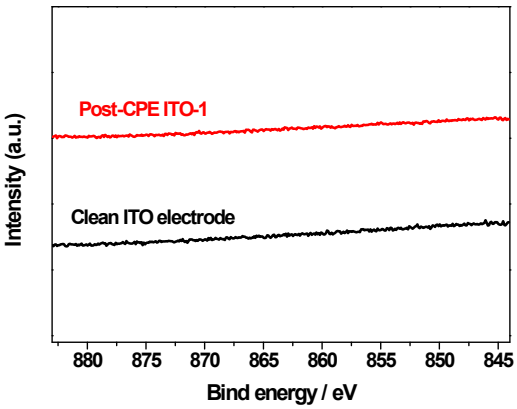

Fig. S17 XPS spectra of Ni element on the surface of clean ITO electrode and post-CPE ITO-**1** electrode. The binding energy has been calibrated by the C 1s peak.

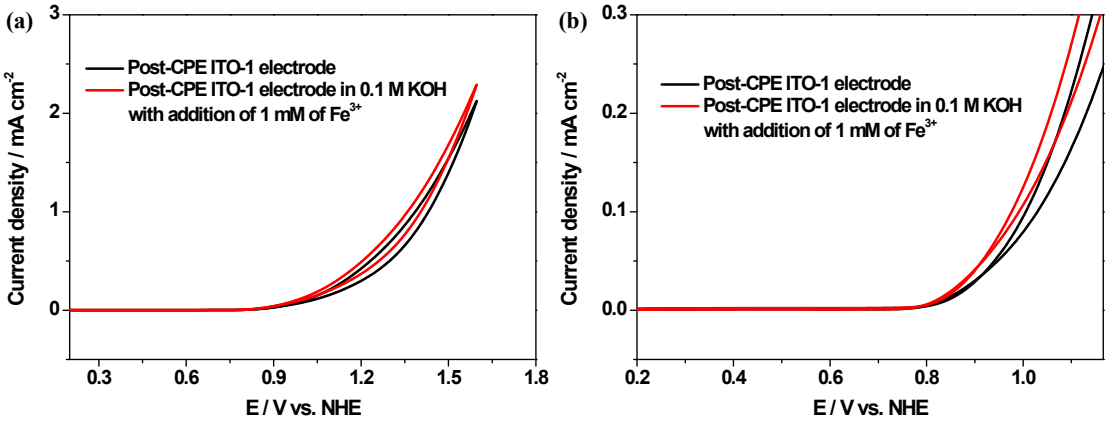

Fig. S18 CV tests of post-CPE ITO-**1** electrode in 0.1 M KOH solution with and without addition of 1 mM Fe^{3+} (a). Enlarged CV curve in low potential region (b).

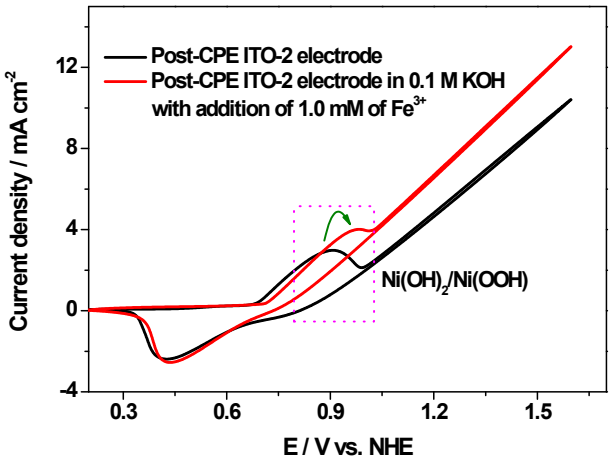

Fig. S19 CV tests of post-CPE ITO-**2** electrode in 0.1 M KOH solution with and without addition of 1 mM Fe^{3+}.

Table S3 Onset overpotential and catalytic current at 1.60 V of **1** and some reported Ni based molecular WOCs.

Catalyst	pH	η/mV [a]	j_{cat} / mA cm^{-2} [b]	v / mV s^{-1} [c]	Ref.
$[Ni(L)(H_2O)_2]^{2+}$	6.5	533	1.5	100	S1
$[Ni^{II}\text{-}L1]^{2+}$	7.0	580	0.5	100	S2
$[Ni(TAML)]^{2-}$	7.0	680	0.7	100	S3
$[NiL]^{2+}$	9.0	550	1.4	100	S4
$[Ni(meso\text{-}L)]^{2+}$	7.0	170	1.2	100	S5
$[Ni(TMC)(CH_3CN)]^{2+}$	7.0	483	1.3	100	S6
$[Ni(mcp)(H_2O)_2]^{2+}$	7.0	480	1.2	100	S7
$[Ni(mabpy)]^{2+}$	7.0	573	0.7	100	S8
$[Ni(bptn)(H_2O)]^{2+}$	9.0	351	0.9	100	S9
$[Ni(mbptn)(CH_3CN)]^{2+}$	9.0	401	0.9	100	S9
$[Ni(tmbptn)(H_2O)]^{2+}$	9.0	581	1.4	100	S9
Ni-PY5	10.8	800	2.5	100	S10
1	7.0	520	2.0	100	This work

[a] η = onset overpotential [b] j_{cat} = current density at 1.60 V vs. NHE [c] Scan rate of CV test for onset overpotential and catalytic current measurement.

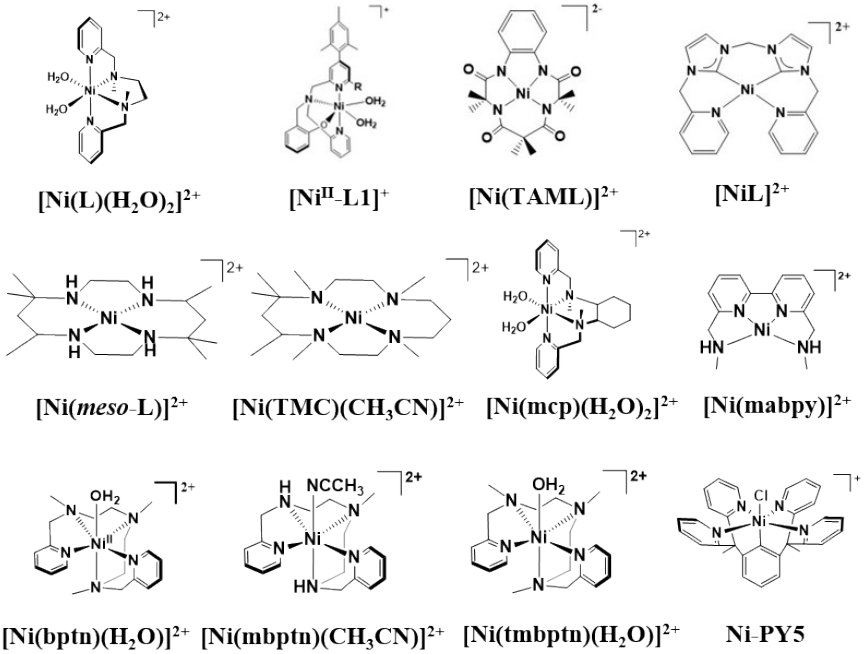

References

[1] G.-Y. Luo, H.-H. Huang, J.-W. Wang, T.-B. Lu, *ChemSusChem*, 2016, **9**, 485–491.

[2] D. Wang and C. Bruner, *Inorg. Chem.*, 2017, **56**, 13638–13641.

[3] H. Lee, X. Wu and L. Sun, *ChemSusChem*, 2020, **13**, 3277–3282.

[4] H. Shahadat, H. Younus, N. Ahmad, M. A. Rahaman, Z. Khattak, S. Zhuiykov and F. Verpoort, *Catal. Sci. Technol.*, 2019, **9**, 5651–5659.

[5] M. Zhang, M.-T. Zhang, C. Hou, Z.-F. Ke and T.-B. Lu, *Angew. Chem., Int. Edit.*, 2014, **53**, 13042–13048.

[6] L. Zhang, F. Yu, Y. Shi, F. Li and H. Li, *Chem. Commun.*, 2019, **55**, 6122–6125.

[7] J.-W. Wang, X-Q.. Zhang, H.-H. Huang and T.-B. Lu, *ChemCatChem*, 2016, **8**, 3287–3293.

[8] Z. Ruan, J. Dong, J. Wang, Z. Qi, X. Chen, X. Liang and J. Lin, *Sustainable Energy Fuels*, 2024, **8**, 1769–1774.

[9] X. Chen, X. Liao, C. Dai, L. Zhu, L. Hong, X. Yang, Z. Ruan, X. Liang and J. Lin, *Dalton Trans.*, 2022, **51**, 18678–18684.

[10] L. Wang, L. Duan, R. Ambre, Q. Daniel, H. Chen, J. Sun, B. Das, A. Thapper, J. Uhlig, P. Dinér and L. Sun, *J. Catal.*, 2016, **335**, 72–78.